Bow Wave Breaking and Viscous Interaction of Stern Wave

Seung-Hyun Kwag*
School of Mechanical Engineering, Halla University

The bow wave breaking and the viscous interaction of stern wave are studied by simulating the free-surface flows. The Navier-Stokes equation is solved by a finite difference method in which the body-fitted coordinate system, the wall function and the triple-grid system are invoked. After validation, the calculations are extended to turbulent flows. The wave elevation at the Reynolds number of 10^4 is much less than that at 10^6 although the Froude number is the same. The numerical appearance of the sub-breaking waves is qualitatively supported by experimental observation. They are also applied to study the stern flow of S-103 for which extensive experimental data are available. Although the interaction between separation and the stern wave generation are not yet clear, the effects of the bow wave on the development of the boundary layer flows are concluded to be significant.

Key Words : Bow Wave Breaking, Viscous Interaction, Stern Wave, Sub-Breaking Phenomena, Finite Difference Method, Triple Grid Scheme, Free Surface Flows

1. Introduction

The free surface flow is one of the most complicated flows where various nonlinear phenomena such as wave breaking, viscous interactions, and free-surface tension exist. There are many experimental studies about the wave breaking such as Duncan(1993), Mori(1985), Grosenbaugh (1988) and, Maruo(1986). In spite the extensive experiments, however, the free-surface nonlinear phenomena still remain unclear. Theoretical investigations have also attempted to explain the phenomena or to provide a suitable model. Dagan(1972) applied instability analysis to predict the breaking. Some models for breaking waves are proposed through experiments. There are some studies on the free-surface tension, [Maruo(1986)]. The stern flows with the free-surface show also important phenomena in ship hydrodynamics. Although Doi(1981) extensively studied them, much remains unclear. Although the viscous interactions are important, theoretical approaches are limited and most of the approaches are based on the simple flow models.

In the present study, the wave breaking and the viscous interaction of the stern waves are studied through numerical simulations. The numerical scheme is based on the MAC method where the body-fitted coordinates and the non-staggered grid system are used. The convection terms are presented by the third-order upstream differencing. The wall function is invoked to follow a steep velocity changes close to the hull in high Reynolds number flows.

2. Numerical Simulation of Ship Waves

2.1 Basic equation

Numerical simulations of 3-D free-surface flows are carried out by using the MAC method. The velocity components u, v and w at (n+1) time step are determined by

$$\begin{aligned} u^{n+1} &= (F^n - \Phi_x^n)\,\Delta t \\ v^{n+1} &= (G^n - \Phi_y^n)\,\Delta t \\ w^{n+1} &= (H^n - \Phi_z^n)\,\Delta t \end{aligned} \tag{1}$$

* **E-mail** : shkwag@hit.halla.ac.kr
TEL : +82-371-760-1233 ; **FAX** : +82-371-762-6705
School of Mechanical Engineering, Halla University, # 66 Heungup, Wonju 220-712, Korea. (Manuscript **Received** August 4, 1999; **Revised** January 17, 2000)

where

$$
\begin{aligned}
F^n=&\frac{u^n}{\Delta t}+\left(\frac{1}{Re}+v_t\right)\nabla^2 u\\
&-\left(u^n\frac{\partial u}{\partial x}+v^n\frac{\partial u}{\partial y}+w^n\frac{\partial u}{\partial z}\right)\\
&-\frac{\partial}{\partial x}\left\{v_t\left(2\frac{\partial u}{\partial x}\right)\right\}-\frac{\partial}{\partial y}\left\{v_t\left(\frac{\partial u}{\partial y}+\frac{\partial v}{\partial x}\right)\right\}\\
&-\frac{\partial}{\partial z}\left\{v_t\left(\frac{\partial u}{\partial z}+\frac{\partial w}{\partial x}\right)\right\}\\
G^n=&\frac{v^n}{\Delta t}+\left(\frac{1}{Re}+v_t\right)\nabla^2 v\\
&-\left(u^n\frac{\partial v}{\partial x}+v^n\frac{\partial v}{\partial y}+w^n\frac{\partial v}{\partial z}\right)\\
&-\frac{\partial}{\partial x}\left\{v_t\left(\frac{\partial v}{\partial x}+\frac{\partial u}{\partial x}\right)\right\}-\frac{\partial}{\partial y}\left\{v_t\left(2\frac{\partial v}{\partial y}\right)\right\}\\
&-\frac{\partial}{\partial z}\left\{v_t\left(\frac{\partial v}{\partial z}+\frac{\partial w}{\partial y}\right)\right\} \qquad (2)\\
H^n=&\frac{w^n}{\Delta t}+\left(\frac{1}{Re}+v_t\right)\nabla^2 w\\
&-\left(u^n\frac{\partial w}{\partial x}+v^n\frac{\partial w}{\partial y}+w^n\frac{\partial w}{\partial z}\right)\\
&-\frac{\partial}{\partial x}\left\{v_t\left(\frac{\partial u}{\partial z}+\frac{\partial w}{\partial x}\right)\right\}\\
&-\frac{\partial}{\partial y}\left\{v_t\left(\frac{\partial v}{\partial z}+\frac{\partial w}{\partial y}\right)\right\}\\
&-\frac{\partial}{\partial z}\left\{v_t\left(2\frac{\partial w}{\partial z}\right)\right\}
\end{aligned}
$$

and

$$\Phi^n=p+\frac{z}{Fn^2} \qquad (3)$$

$$\nabla^2=\frac{\partial}{\partial x^2}+\frac{\partial}{\partial y^2}+\frac{\partial}{\partial z^2} \qquad (4)$$

Differentiating Eq. (1) with respect to x, y and z,

$$
\begin{aligned}
\nabla^2\Phi=&F_x+G_y+H_z\\
&-(u_x^{n+1}+v_y^{n+1}+w_z^{n+1})/\Delta t
\end{aligned} \qquad (5)
$$

The last term in Eq. (5) is expected to be zero to satisfy the continuity condition. Eq. (5) can be solved by the relaxation method. The new free-surface at the (n+1)th time-step is calculated by moving the marker particles by

$$
\begin{aligned}
x^{n+1}&=x^n+u^n\Delta t\\
y^{n+1}&=y^n+v^n\Delta t\\
z^{n+1}&=z^n+w^n\Delta t
\end{aligned} \qquad (6)
$$

It is desirable to introduce coordinate transformations which simplify the computational domain in the transformed domain

$$\xi=\xi(x, y, z),\ \eta=\eta(x, y, z),\ \zeta=\zeta(x, y, z) \qquad (7)$$

Through transformations, Eq. (1) can be written,

$$
\begin{aligned}
q_t+Uq_\xi+Vq_\eta+Wq_\zeta=&\left(\frac{1}{Re}+v_t\right)\nabla^2 q\\
&-K-REYSF(\xi, \eta, \zeta)
\end{aligned} \qquad (8)
$$

where U, V and W are the contravariant velocities and K is the pressure gradient.

2.2 Triple-grid method

Three mesh systems are used whose sizes are different from each other depending on the characteristic of equations. It is called the triple-grid method. The first one is for the convective terms in the N-S equation, the second is for the Poisson equation, and the third is for the free surface equation. The third grid system requires the finest one-four times as large as the first one in the grid number at each direction. According to the results, the prediction of free surface elevation is strikingly improved. The CPU time and the memory size of the present computation are relatively small owing to the use of coarse meshes of the second mesh system for the Poisson equation and the diffusion term (Xu, 1989).

2.3 Computational result and discussion

Computations are performed for flow fields around the Wigley model with free surface at Re $=10^4$ and 10^6. Figure 1 shows the view of the grid scheme. The grid number is $74\times29\times19$. During the computation, the location of grids between the free surface and the bottom is redistributed proportionally to the free surface elevation. Through this scheme, it is expected that the free-surface condition (i. e., the constant pressure condition) can be directly applied without any interpolation. For high Reynolds number flows, the two-layer algebraic Baldwin-Lomax model is used for eddy viscosity. The numerical results are compared

Fig. 1 View of grid scheme

with the experimental data (IHI, 1983).

In order to check the convergence of computations, the wave patterns and drag coefficients C_p, C_f, and C_w are compared along the marching time step in Fig. 2. Here C_p, C_f, and C_w represent the drag coefficients for pressure, friction and wave-making. Schoenherr friction line and the measured (IHI, 1983) wave-making resistance coefficient are shown for comparison. Although the wave seems still developing further, it can be assumed to be converged at t=3.0. The calculated frictional resistance, which is directly derived by the difference of the velocities at the two points, is still larger than the Schoenherr's prediction. Figure 3 shows the logarithmic plot of velocity at x/L=0.835 (u^+ versus y^+) using the friction velocity. Some plots are drawn at several points in the girth and depth-wise directions. They are generally in good agreement. Figure 4 shows the comparison of the velocity distribution near the wall between those obtained by making use of the law-of-the-wall and those measured directly. Since the wall-function may not be valid for separated flows, it is not applied in the stern 5% where separation is suspected. There the scheme is switched to the direct method which employs more grids in the boundary layer instead of using the wall function. Usually it is not easy to use so many grids within the boundary layer for separated flows, especially at high Reynolds number, due to the computer's memony capability. According

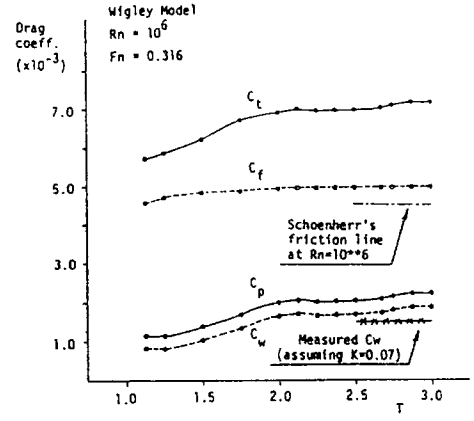

Fig. 2 Time history of drag coefficient

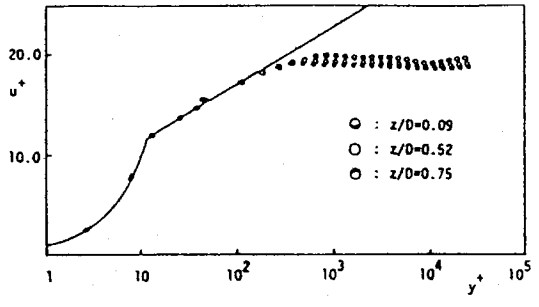

Fig. 3 Log plot of velocity for Wigley model

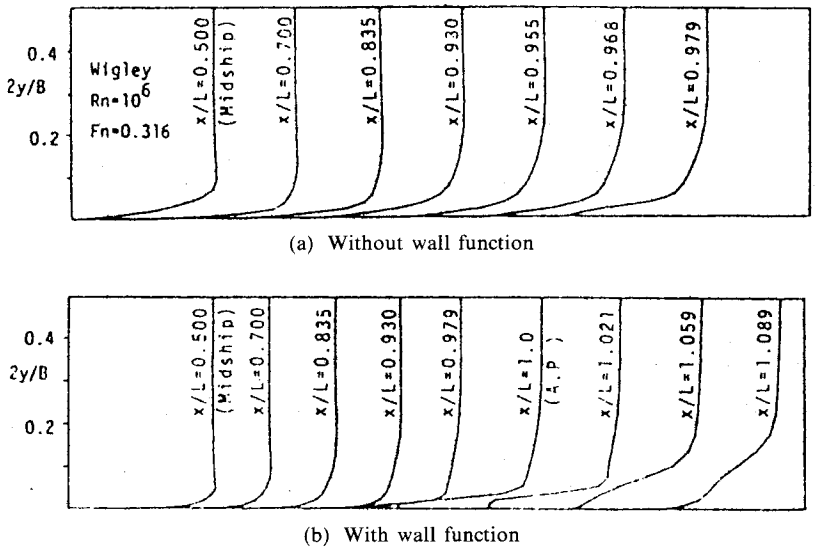

(a) Without wall function

(b) With wall function

Fig. 4 u-velocity distribution on free surface

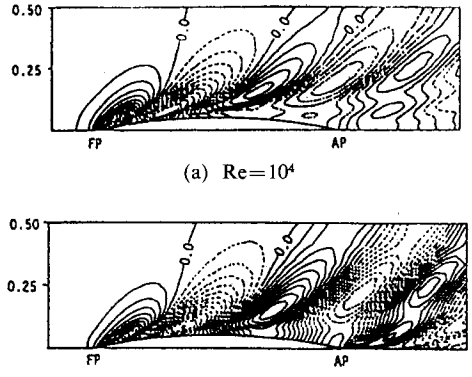

Fig. 5 Wave patterns of Wigley model

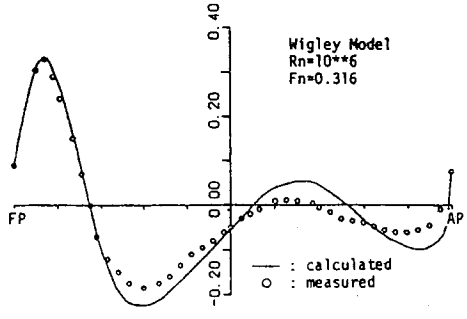

Fig. 6 Wave profile on hull surface, measured data (IHI, 1983)

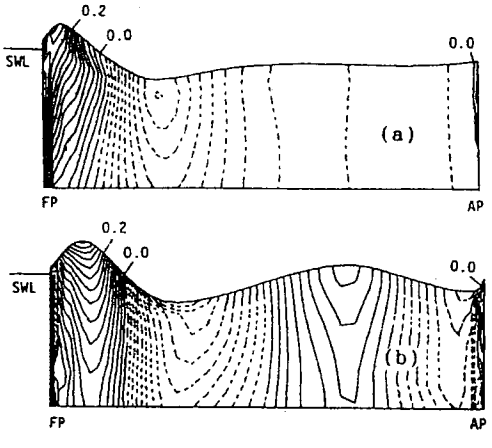

Fig. 7 Pressure contour on hull surface (a) Re=10⁴ (b) Re=10⁶

to the results, the steep velocity gradients near the hull are well captured even with a limited number of grids. Figure 5 shows the comparison of the wave patterns at Re=10⁴ and 10⁶. We can clearly see the Reynolds number dependency of the wave.

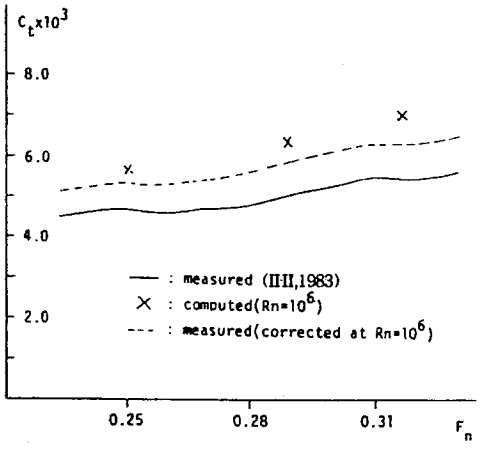

Fig. 8 Comparison of total drag coefficients

It may confuse us that even the second wave crest differs much in height, for we usually expect the Reynolds number effect on waves to be insignificant. Figure 6 shows the wave profile along the hull surface. The Reynolds number of the measurement is 3.59×10^6. It is well predicted around the bow, but slight discrepancies are still observed in the aft half of the hull. Figure 7 shows the pressure contours on the hull surface at Re=10^4 and 10^6. The pressure around the stern region is recovered more at 10^6 than at 10^4. The pressure distribution on the hull surface shows some wiggles in appearance at the bow and stern parts due to the use of a coarse mesh. However, the wave height on free surface, which means the pressure here, shows no serious wrinkles because a finer grid is used there. In Fig. 8, calculated and measured total drag coefficients are shown. The calculations are for Re=10^6. The Reynolds numbers of measurements were made Reynolds numbers 2.84×10^6, 3.28×10^6, and 3.59×10^6 for the corresponding Froude number of 0.25, 0.289 and 0.316, respectively. For a more direct comparison, the measured results are corrected to the Reynolds number of 10^6 through the Prandtl-Schlichting's friction formula. The computed drag is still greater than the experimental data. We cannot mention the reason for the difference conclusively. However, the accuracy of the velocity calculation close to the hull may be insufficient resulting in a poor agreement in the frictional resistance.

3. Detection of Sub-Breaking Waves

3.1 Appearing condition of sub-breaking

Computed results are applied to detect the appearance of sub-breaking waves around bow. The critical condition for their appearance was studied by Mori(1989). The breaking at their infant stage is concluded to be a free-surface turbulent flow. It is supposed that the surplus energy accumulated around the wave crest by the increment of the free surface could eventually maintain itself without any overturning or backward flows. An instability analysis provides a critical condition for their appearance;

$$\frac{M}{U_s}\frac{\partial M}{h\partial s}-\frac{1}{n_z}\frac{\partial n_z}{h\partial s}>0 \tag{9}$$

where M is the circumferential force given by

$$M=(KU_s^2-n_zg)\,n_z \tag{10}$$

s is the stream line coordinate along the free-surface and h is its metric coefficient. The normal coordinate is denoted by n, and n_z is the direction cosine of n to z. U_s is the velocity component of basic flow in the s-direction; K is the curvature of the free surface and g is the gravity acceleration. Limiting ourselves to a narrow region close to the wave crest, we assume $n_z \fallingdotseq 1$ and $\partial/h\partial s \fallingdotseq \partial/\partial x$. Then Eq. (9) can be reduced approximately into

$$\frac{U_s^2}{M}\frac{\partial}{\partial x}\frac{M}{U_s}>0 \tag{11}$$

where,

$$M=KU_s^2-g \tag{12}$$

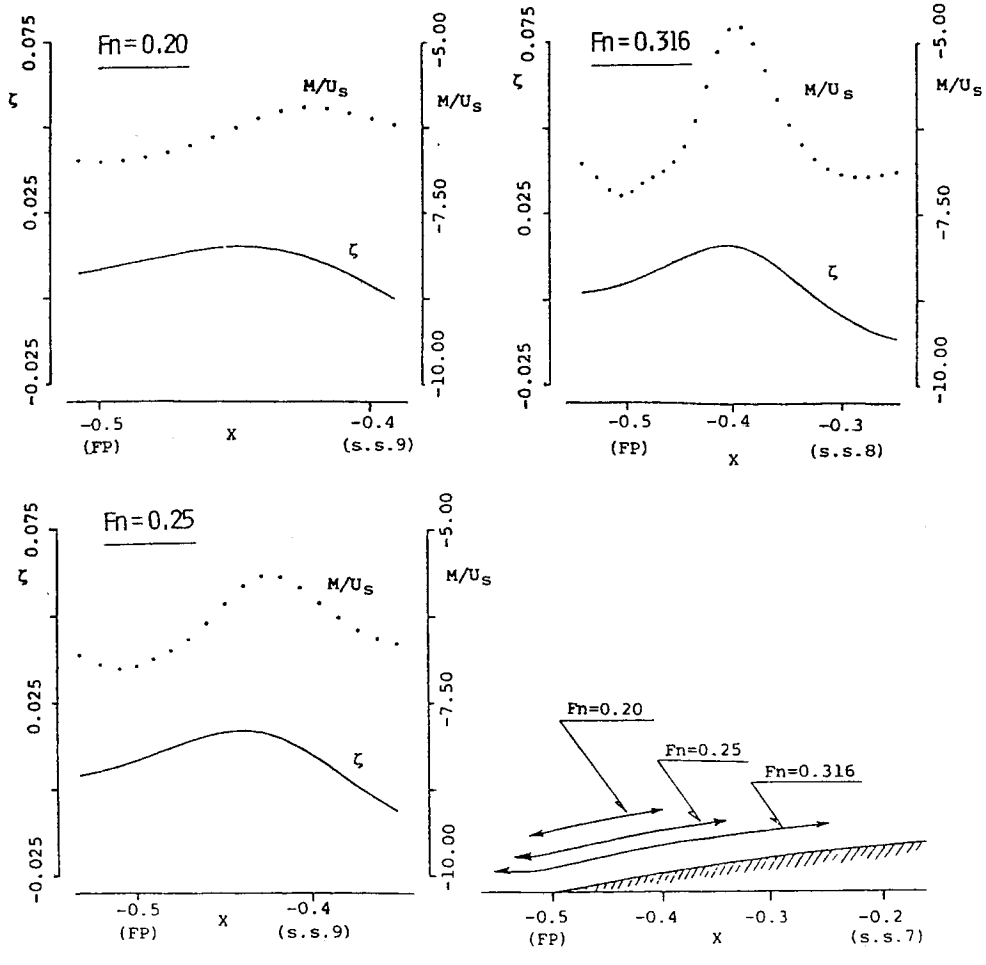

Fig. 9 Variation of M/Us and free surface elevation and lines analysis

Because M is always negative, the negative gradient of M/U_s to x suggests possibilities for free surface flows to be unstable.

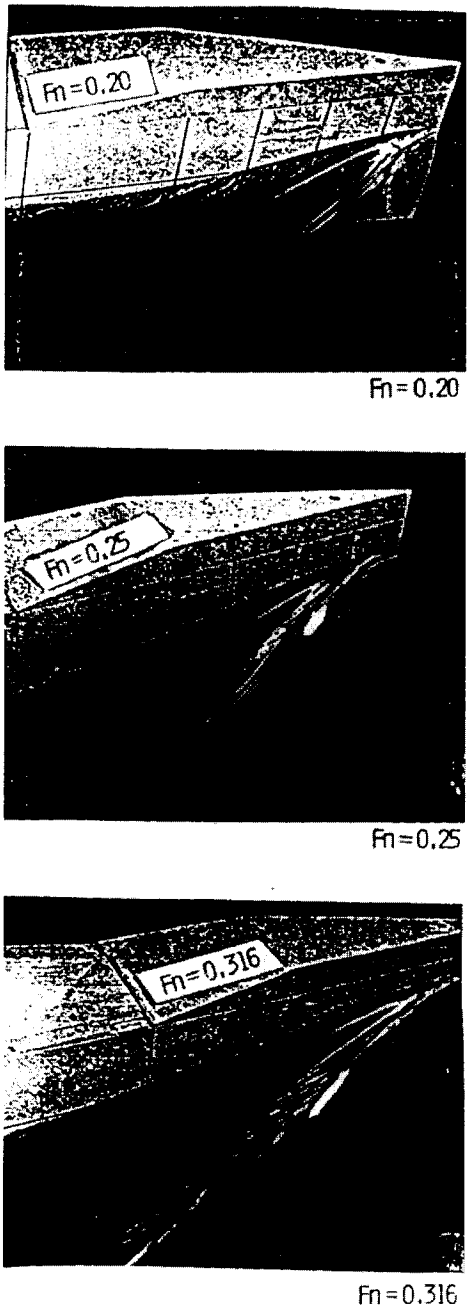

Fig. 10 Photos of wave profiles for Wigley model, taken at Hiroshima Univ. Circulating water channel

3.2 Numerical application for bow wave

The appearing condition is numerically simulated to predict the ship wave sub-breaking by Eq. (11). Figure 9 shows the variations of M/U_s vs x around the first bow wave crest. The analyses are made at the three speeds of Fn=0.20, 0.25 and 0.316. The free surface elevation is denoted by ζ. At Fn=0.20, no steep negative gradient is seen, but the gradients at Fn=0.25 and 0.316 are negative behind the wave crest. It may be suggested that the free surface flows at Fn=0.20 is stable. Figure 10 shows the photographs of the free-surface flows taken at the three corresponding Froude numbers. Wrinkle-like waves behind the diverging waves at Fn=0.25 and 0.316 can be seen. Those at Fn=0.316 are much more intensive than those at Fn=0.25. On the contrary, no such waves can be observed at Fn=0.20. This observation supports the instability analysis for the bow wave breaking.

4. Discussion on Stern Waves

The viscous interaction of stern wave of S-103 is studied through simulation. S-103 is an Inuid model with the beam/length ratio of 0.09 on which extensive experiments have been carried out by Doi (1981). Figure 11 shows the calculated and measured wave profiles along the hull surface at Fn=0.30. The computed profile shows

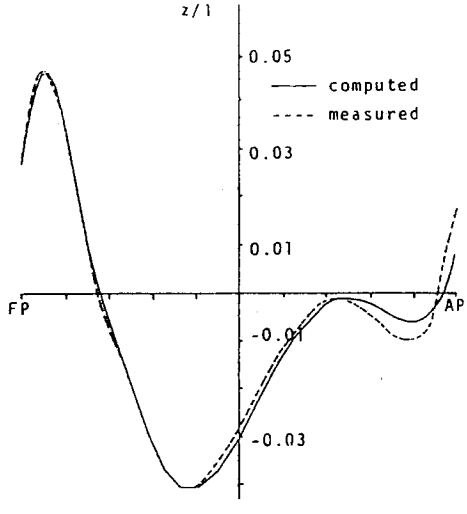

Fig. 11 Comparison of wave profile of S103

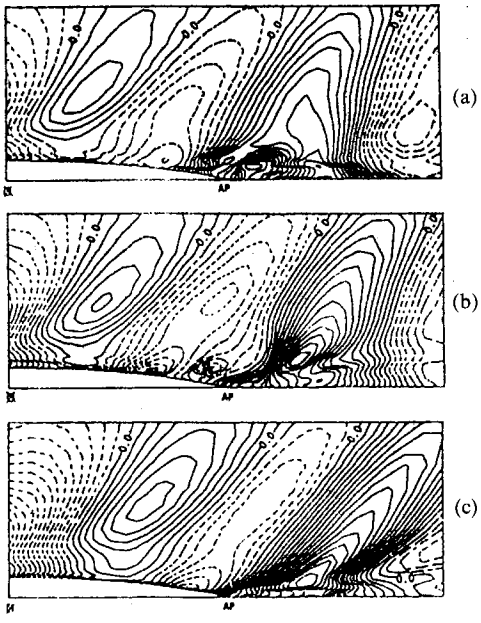

Fig. 12 Stern wave patterns of S103
(a) Fn=0.27 (b) 0.28 (c) 0.30
(Contour Interval $0.02\times 2g\zeta/U_0^2$)

a good agreement with the measured one. Thus, the present numerical scheme works well and the results may endure for our purpose to discuss on the flow mechanism.

4.1 Discussion on viscous interaction

Figure 12 shows the computed stern wave patterns at the three Froude numbers of 0.27, 0.28 and 0.30. Comparing the first stern wave crests, we can see that the result of Fn=0.27 looks different from the others. It differs from that of Fn =0.28 although the difference in the speed is not so large. The stern wave crest of Fn=0.27 is not clear. This may agree qualitatively with the observed. On the other hand, the crest of Fn=0.30 is rather sharp and large. The modest elevation of the stern wave at Fn=0.27 may be related to the development of the boundary layer and separation.

4.2 Detection of sub-breaking

Figure 13 shows the measured (Doi, 1981) and computed wave profiles and velocity vectors of Fn=0.30. The measured free surface fluctuates intensively around the crest (indicated by I there).

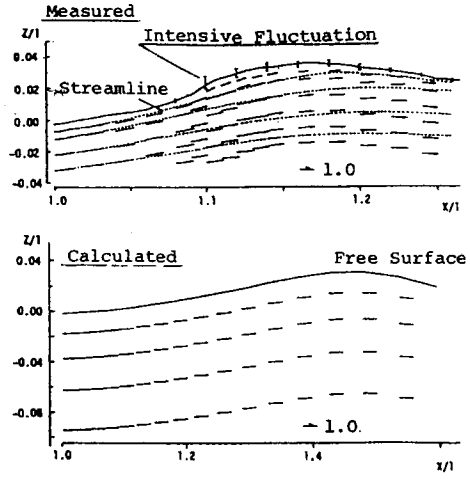

Fig. 13 Wave profile and velocity vector (x-z plane, y/l=0.15 for S103)

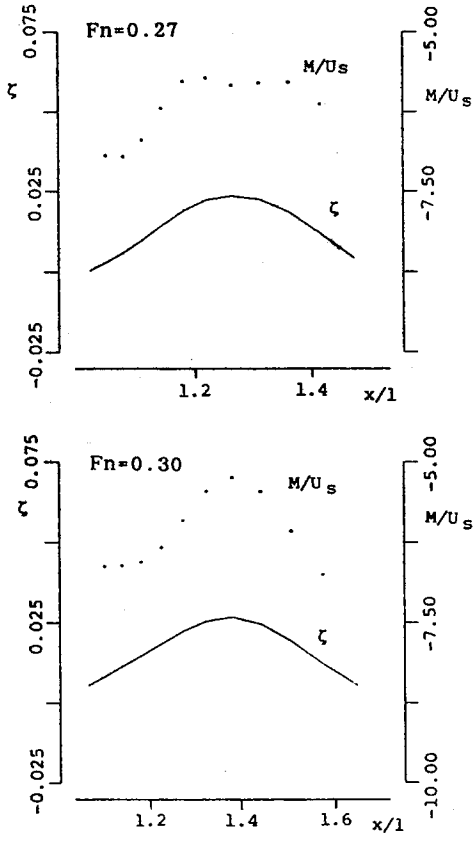

Fig. 14 Variation of M/U_s and free surface elevation and lines analysis of S103

The calculated free surface is steady because no special attention to the sub-breaking is paid in

the calculation. It should be pointed out that the measured wave crest is upstream of the calculated crest. The detection of the appearance of sub-breaking waves is made for the stern waves at Fn =0.27 and 0.30. The values of M/U_s are calculated along y/l=0.09 and are shown in Fig. 14. A steep negative gradient is seen at Fn=0.30 but not at Fn=0.27. This means that the wave crest at Fn =0.30 can be subject to sub-breaking but not at Fn=0.27. It is concluded that the bow wave affects much on the separation and eventually the stern wave generation appreciably. The appearance of sub-breaking wave makes the flow field completely different and it may be necessary to include them in the computation.

5. Conclusions

(1) A numerical scheme is developed to simulate 3-D free surface flows at high Reynolds numbers. Steady-state solutions can be obtained with monotonic convergency. The triple grid method is applied to get well-developed free surface waves within a moderate computer's memory.

(2) The Reynolds number effects on waves are especially significant on the stern wave and pressure distribution in the aft part of the hull. The calculated resistance is greater than the measured. The estimation of the frictional resistance is still a source of over-estimation.

(3) The criterion for the appearance of sub-breaking waves works well, and the present numerical scheme can be applied to predict breaking of ship waves. The results are supported by experiment.

(4) The stern wave is affected by the separation of the boundary layer flow which may be under the influence of the bow wave. The occurrence of sub-breaking changes the flow fields drastically, especially for the stern waves.

References

Dagan, G. and Tulin, M. P., 1972, "Two Dimensional Free-Surface Gravity Flow past Blunt Bodies," *Jour. Fluid Mech.*, Vol. 51, Part 3

Doi, Y., Kajitani, H., Miyata, H. and Kuzumi, S., 1981, "Characteristics of Stern Waves generated by Ships of Simple Hull Form(1st Report)," *Jour. of Soc. of Naval Arch. of Japan*, Vol. 150

Duncan, J. H., 1993, "The Breaking and Non-breaking Wave Resistance of a Two-Dimensional Hydrofoil," *Jour. Fluid Mech.*, Vol. 126

Grosenbaugh, M. A. and Yeung, R. W., 1988, "Non-linear Bow Flows — An Experimental and Theoretical Investigation," *Proc. of 17th Symp. on Naval Hydro.*

IHI, SRI, UT, YNU, 1983, *Cooperative Experiments on Wigley Parabolic Models in Japan*, prepared for the ITTC Resistance Committee, 2nd edition

Maruo, H. and Ikehata, M., 1986, "Some Discussions on the Free Surface Flow around the Bow," *Proc. of 16th Symp. on Naval Hydro.*

Mori, K. and Doi, Y., 1985, *Flow Characteristics of 2-Dimensional Sub-Breaking Waves, turbulence Measurements and Flow Modeling*, Hemisphere Pub. Co.

Mori, K. and Shin, M. S., 1989, "Sub-Breaking Wave : Its Characteristics, Appearing Condition and Numerical Simulation," *Proc. of 17th Symp. on Naval Hydro.*

Xu, Q., Mori, K. and Shin, M., 1989, "Double-Mesh Method for Efficient Finite-Difference Calculations," *Jour. of the Soc. of Naval Arch. of Japan*, Vo. 166